

Robust and Deterministic Preparation of Bosonic Logical States in a Trapped Ion

V. G. Matsos^{1,2}, C. H. Valahu^{1,2,3}, T. Navickas,^{1,2} A. D. Rao,^{1,2} M. J. Millican,^{1,2} X. C. Kolesnikow^{1,2}, M. J. Biercuk,^{1,2} and T. R. Tan^{1,2,3,*}

¹School of Physics, University of Sydney, New South Wales 2006, Australia

²ARC Centre of Excellence for Engineered Quantum Systems, University of Sydney, New South Wales 2006, Australia

³Sydney Nano Institute, University of Sydney, New South Wales 2006, Australia



(Received 12 November 2023; accepted 10 June 2024; published 30 July 2024)

Encoding logical qubits in bosonic modes provides a potentially hardware-efficient implementation of fault-tolerant quantum information processing. Here, we demonstrate high-fidelity and deterministic preparation of highly nonclassical bosonic states in the mechanical motion of a trapped ion. Our approach implements error-suppressing pulses through optimized dynamical modulation of laser-driven spin-motion interactions to generate the target state in a single step. We demonstrate logical fidelities for the Gottesman-Kitaev-Preskill state as high as $\bar{F} = 0.940(8)$, a distance-3 binomial state with an average fidelity of $F = 0.807(7)$, and a 12.91(5) dB squeezed vacuum state.

DOI: 10.1103/PhysRevLett.133.050602

Fault-tolerant quantum error correction (QEC) for quantum information processing necessitates the implementation of redundant encoding within a sufficiently large Hilbert space to yield protection against local hardware errors [1]. At present, the predominant strategy focuses on encoding a logical qubit with multiple discrete-variable physical qubits manipulated with ultralow operational errors [2,3]. This approach is resource intensive, and, despite many impressive demonstrations [4–9], the viability of using QEC in this way to deliver net improvements in hardware error rates remains challenging. Many analyses indicate that a large ratio of physical-to-logical qubits is necessary for fault-tolerant operation in target algorithms, posing a substantial resource penalty and far outstripping device sizes available in the near future [10]. An alternative approach involves encoding logical qubits within continuous-variable systems [11,12]. In particular, the infinite-dimensional Hilbert space spanned by the bosonic mode of a harmonic oscillator offers a highly symmetrical physical system that lends itself to logical encodings including Gottesman-Kitaev-Preskill (GKP) [13], binomial [14], and cat [15] codes. This approach demands fewer individual physical devices at the cost of increased complexity in preparing and controlling the logical code words.

Several experimental works have successfully created different classes of bosonic logical states [16–21], implemented logical gate sets [22], and demonstrated QEC protocols [23–29]. However, preparing high-quality bosonic codes for use in QEC remains a significant challenge. For instance, attaining fault tolerance by concatenating the GKP code with discrete-variable error-correcting codes requires a

squeezing parameter currently estimated at approximately 10 dB [30,31], a threshold yet to be experimentally reached. Additionally, only the lowest-order binomial code words (distance-2) have been experimentally realized so far, while a minimum distance of 3 is necessary to correct all types of bosonic errors [14].

In this work, we experimentally demonstrate high-fidelity deterministic preparation of a variety of bosonic states by integrating concepts of error suppression via robust control into the protocol for QEC encoding. Code word generation is achieved in a single step using optimized time-domain modulation of the control fields used to manipulate the qubit and motional modes of a trapped ion. The control pulses, obtained from a numerical optimizer, are designed to exhibit robustness against motional dephasing [32]. We demonstrate the versatility of our approach by creating several classes of bosonic states: a highly squeezed 12.91(5) dB state; square and hexagonal GKP states with a logical fidelity and squeezing as high as 0.940(8) and 7.5(2) dB, respectively; and the first realization of a distance-3 binomial logical state that can simultaneously protect against universal (correctable) bosonic errors. Finally, we demonstrate the robustness of our protocol to systematic imperfections by demonstrating up to 4.8× lower error than nonrobust solutions in the presence of quasistatic motional-frequency offsets.

State-preparation is implemented by laser-induced spin-boson interactions for a single trapped ion described by the effective Hamiltonian

$$\hat{H}(t) = \frac{\Omega_r(t)}{2} \hat{\sigma}^+ \hat{a} e^{i\phi_r(t)} + \frac{\Omega_b(t)}{2} \hat{\sigma}^+ \hat{a}^\dagger e^{i\phi_b(t)} + \text{H.c.}, \quad (1)$$

where $\hat{\sigma}^+ = |\uparrow\rangle\langle\downarrow|$ is the raising operator of the qubit and \hat{a} (\hat{a}^\dagger) is the annihilation (creation) operator of the oscillator.

*Contact author: tingrei.tan@sydney.edu.au

The two terms in the Hamiltonian are referred to as the red-(RSB) and blue-sideband (BSB) interactions [33] with their respective time-dependent Rabi rates, $\Omega_{r,b}(t)$, and phases, $\phi_{r,b}(t)$. This Hamiltonian provides sufficient control to produce the bosonic states considered in this work, where the required nonlinearities for these states are generated from noncommuting terms in the Hamiltonian at different times [34]. Furthermore, universal control of the qubit-oscillator system may be obtained through the addition of a carrier interaction $\hat{H}_c(t) = \Omega_c(t)\hat{\sigma}^+e^{i\phi_c(t)}/2 + \text{H.c.}$ [19,43], but is not necessary to prepare the states considered in this Letter.

We numerically design the time-dependent controls of $\hat{H}(t)$ such that a target bosonic state is created via the time evolution operator $e^{-i\int \hat{H}(t)dt}$ with $\{\Omega_{r,b}(t), \phi_{r,b}(t)\}$ as optimizable control parameters. Optimized control pulses are obtained through a gradient-based constrained optimization using Q-CTRL's Boulder Opal package [32,44]. Constraints are included on candidate control pulses to improve experimental implementation: first, the Rabi rates of the RSB and BSB interactions are kept constant throughout the evolution [$\Omega_r(t) = \Omega_b(t) = 2\pi \times 2$ kHz] to avoid unwanted time-varying Stark shifts; second, slew-rate and filtering constraints are added to the optimized waveform phases to comply with hardware limitations. We define the cost function to maximize pulse fidelity for a target state-preparation task in the presence of motional dephasing (the dominant source of noise in our system) while also minimizing total pulse durations [34].

Our experiment is performed with a single $^{171}\text{Yb}^+$ ion confined in a macroscopic Paul trap, with radial frequencies $\{\omega_x, \omega_y\} = 2\pi \times \{1.33, 1.51\}$ MHz. The bosonic states are encoded in the radial- x mode, while the ancillary qubit is made up of the two magnetically insensitive hyperfine levels of the $^2\text{S}_{1/2}$ ground state with $|\downarrow\rangle = |F=0, m_F=0\rangle$ and $|\uparrow\rangle = |F=1, m_F=0\rangle$. Coherent spin-motion interactions are enacted by a 355 nm pulsed laser through stimulated Raman transitions. Phase modulation of the RSB and BSB interactions is implemented by adjusting a radio-frequency (rf) signal that drives an acousto-optic-modulator in the path of the Raman beam (see Refs. [45,46] for more details on the experimental system).

The experimental pulse sequence used in *state-preparation* is shown in Fig. 1; after initializing the qubit and bosonic mode to their ground state, $|\downarrow\rangle \otimes |0\rangle$, we apply the Hamiltonian of Eq. (1) with the numerically optimized pulses to prepare the target state $|\downarrow\rangle \otimes |\psi\rangle$. This is followed by a *state reconstruction* protocol that aims to retrieve the density matrix of the experimentally generated state. To this end, we measure the characteristic function

$$\chi(\beta) = \langle \hat{D}(\beta) \rangle, \quad (2)$$

where $\hat{D}(\beta) = e^{\beta\hat{a}^\dagger - \beta^*\hat{a}}$ is the displacement operator and $\beta \in \mathbb{C}$ is a point in phase space.

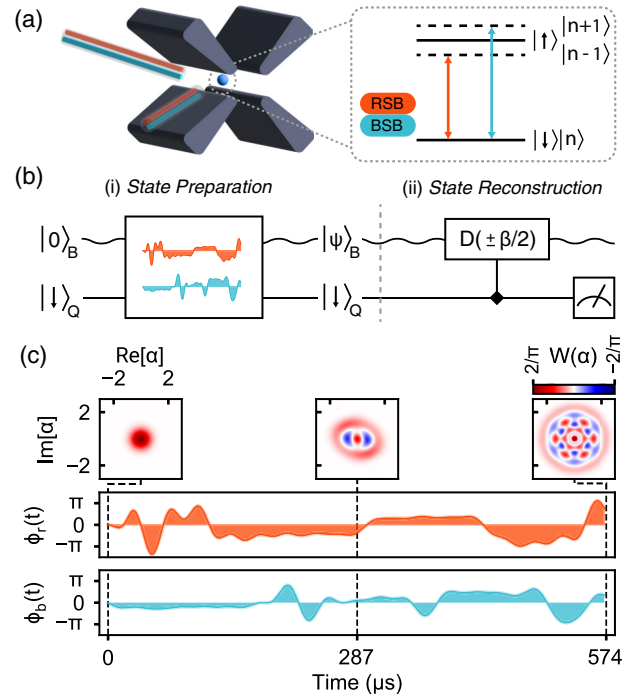


FIG. 1. State preparation of nonclassical bosonic states in an ion trap. (a) Two orthogonal Raman beams couple the spin and motion of a trapped ion, inducing spin-dependent forces. (b) Experimental pulse sequence: (i) the bosonic mode and qubit are initialized to their ground state; the control pulse evolves the system to the target bosonic state under $\hat{H}(t)$ [Eq. (1)]. (ii) Reconstruction of characteristic function, $\chi(\beta)$, by applying a displacement, $\hat{D}(\pm\beta/2)$, conditioned on the qubit state in the $\hat{\sigma}_x$ basis. Readout of the ancilla qubit in the $\hat{\sigma}_z$ basis measures $\text{Re}[\chi(\beta)]$. (c) Target bosonic states are prepared by modulating $\phi_{r,b}(t)$ of the bichromatic fields. Insets show the time evolution of the Wigner function for the $(|0\rangle + \sqrt{3}|6\rangle)/2$ binomial state.

The characteristic function is sampled using the protocol outlined in [47]. We apply a state-dependent force (SDF) $\hat{D}[\beta(t)\hat{\sigma}_x/2]$, where $\beta(t)/2 = \Omega t e^{-i(\phi_r - \phi_b)/2}/2$, which maps information from the bosonic mode onto the qubit for readout. The SDF is implemented by simultaneously applying the RSB and BSB interactions with $\Omega_r = \Omega_b = \Omega$. The real part of the characteristic function, $\text{Re}[\chi(\beta)]$, is determined through projective readout of the internal qubit state of the ion (the imaginary part of the characteristic function can be obtained by applying a qubit rotation prior to the SDF). We only perform measurements in the positive quadrant of phase space. For the states considered in this work, the remaining quadrants are obtained in postprocessing by the symmetry of $\chi(\beta)$ with respect to both phase space axes. Furthermore, we only reconstruct $\text{Re}[\chi(\beta)]$ as the imaginary part vanishes under this same symmetry.

We experimentally generate several bosonic states to demonstrate the versatility of our protocol. Each state is prepared by implementing a targeted control solution obtained from the numerical optimizer with results

TABLE I. Fidelities, squeezings, and durations of experimentally prepared bosonic states. The state-preparation fidelities, defined as $\mathcal{F} = \langle \psi_t | \hat{\rho}_{\text{exp}} | \psi_t \rangle$, are calculated from the reconstructed density matrices $\hat{\rho}_{\text{exp}}$ of the data in Figs. 2 and 3. We also report the logical fidelities of the GKP states, denoted by the subscript L. Uncertainties correspond to the 1-sigma deviation obtained from bootstrapping.

State	Fidelity	Squeezing (dB)	Time (μs)
$\hat{S}(r = 1.55) 0\rangle$	0.753(4)	12.91(5)	1057
$\text{GKP}_{\Delta=0.247}^s$	0.90(1)_L, 0.60(1)	5.5(2), 6.3(2)	1301
$\text{GKP}_{\Delta=0.301}^s$	0.940(8)_L, 0.83(1)	7.5(2), 7.5(2)	933
$\text{GKP}_{\Delta=0.301}^h$	0.91(1)_L, 0.77(3)	6.5(3), 6.3(4)	978
$(0\rangle + 4\rangle)/\sqrt{2}$	0.889(9)	...	514
$(0\rangle + \sqrt{3} 6\rangle)/2$	0.843(9)	...	688
$(\sqrt{3} 3\rangle + 9\rangle)/2$	0.77(1)	...	780

summarized in Table I. The density matrix, $\hat{\rho}_{\text{exp}}$, is retrieved from the experimentally measured characteristic function using a convex optimization procedure [34,48]. State-preparation fidelity is then computed as $\mathcal{F} = \langle \psi_t | \hat{\rho}_{\text{exp}} | \psi_t \rangle$, where $|\psi_t\rangle$ is the target state. For GKP states, we also report the logical fidelity that quantifies the amount of logical information contained in the state [49]. We bootstrap these measurements to determine the associated uncertainties [50].

We first prepare a squeezed state $\hat{S}(r)|0\rangle$, where $\hat{S}(r) = \exp[\frac{1}{2}(r^* \hat{a}^2 - r \hat{a}^{\dagger 2})]$, with a target squeezing parameter of $r = 1.55$. The reconstructed characteristic function is

shown in Fig. 2(a), which we fit to theory [47] and find a squeezing parameter $r = 1.487(5)$ [12.91(5) dB]. We detail squeezing estimations using multiple analysis methods in the Supplemental Material [34]. We determine a fidelity of 0.753(4), where the accuracy is limited by motional dephasing during reconstruction.

We next prepare approximate GKP code words (see the Supplemental Material [34] for a detailed description). The exact GKP codespace is defined as the mutual +1 eigenspace of the stabilizer displacement operators $\hat{S}_X = \hat{D}(2\alpha)$ and $\hat{S}_Z = \hat{D}(2\beta)$, for $\beta\alpha^* - \beta^*\alpha = i\pi$ and $\alpha, \beta \in \mathbb{C}$. This definition admits unphysical GKP code words whose Wigner functions are two-dimensional grids of delta functions with infinite extent. GKP states can be made physical by applying a Gaussian envelope characterized by the parameter $\Delta \in [0, 1]$, where the exact code words are recovered in the limit $\Delta \rightarrow 0$ [13].

We prepare the $|0\rangle_L$ logical states of a square and a hexagonal GKP code with target squeezings of 10.43 dB ($\Delta = 0.301$), and an additional square GKP code with 12.15 dB ($\Delta = 0.247$) [see Figs. 2(c)–2(h)]. The preparation of $|1\rangle_L$ states is not shown experimentally; however, our pulse optimization scheme produces similar results in fidelity and duration. The state-preparation fidelity, \mathcal{F} , and logical fidelity, \mathcal{F}_L [34], are reported in Table I.

The achieved squeezings of the GKP states are calculated from $\hat{\rho}_{\text{exp}}$ with $\langle \hat{S}_X \rangle$ and $\langle \hat{S}_Z \rangle$, as defined in Ref. [51] (see Table I). Alternatively, using the

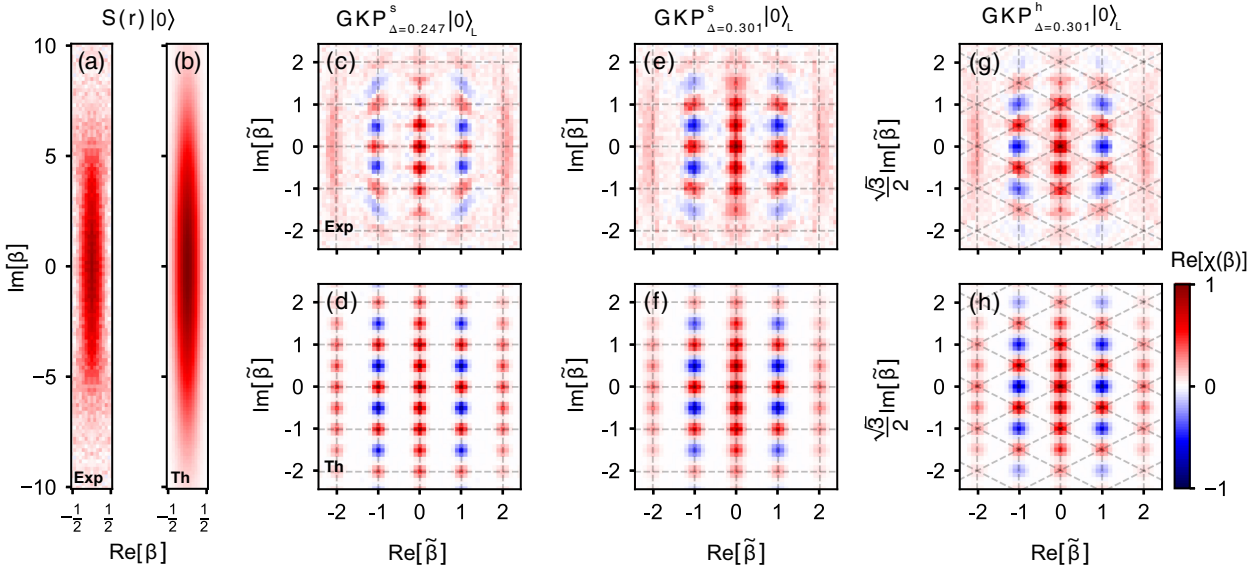


FIG. 2. Experimentally reconstructed characteristic functions of squeezed and GKP states. (a),(b) Squeezed state with a target squeezing parameter $r = 1.55$ created with only coherent first-order sideband interactions. (c)–(f) Approximate square GKP states with target envelope parameters of $\Delta = 0.247$ and $\Delta = 0.301$, respectively. (g),(h) Approximate hexagonal GKP state with target $\Delta = 0.301$. The theoretical characteristic functions of each GKP state are plotted below each subfigure. The phase space coordinates are normalized with $\tilde{\beta} = \beta/\sqrt{2\pi}$ for the square and $\tilde{\beta} = \beta/\sqrt{\sqrt{3}\pi}$ for the hexagonal GKP plots. The achieved fidelities, squeezing levels, and pulse durations are summarized in Table I. The theoretical decoherence-free fidelities are $\mathcal{F}_{\text{th}} \geq 0.99$ for the squeezed state and $\mathcal{F}_{\text{th}} \geq 0.975$ for the GKP states. We attribute the circular smearing in (c) and (e) to motional mode dephasing.

analysis method of Ref. [19] results in squeezings of $\{GKP_{\Delta=0.247}^s, GKP_{\Delta=0.301}^s, GKP_{\Delta=0.301}^h\} = \{10.4(1), 9.47(8), 9.1(1)\}$ dB, which are considerably higher than the values calculated above. The discrepancy in the results obtained by the two methods motivates a more comprehensive characterization method for GKP states (a discussion on these methods is included in the Supplemental Material [34]).

We also prepare binomial code words, which encode logical qubits in finite superpositions of Fock states [14] (see the Supplemental Material [34] for a detailed description). Binomial codes can exactly correct for errors that are polynomial in creation and annihilation operators [52]. We first create the state $|+Z_{S=1}\rangle_{\text{bin}} = (1/\sqrt{2})(|0\rangle + |4\rangle)$ [see Figs. 3(a)–3(c)], which can protect against linear errors in \hat{a} or \hat{a}^\dagger . We then create distance-3 binomial states, $|+Z_{S=2}\rangle_{\text{bin}} = \frac{1}{2}(|0\rangle + \sqrt{3}|6\rangle)$ and $|+Z_{S=2}\rangle_{\text{bin}} = \frac{1}{2}(\sqrt{3}|3\rangle + |9\rangle)$ [see Figs. 3(d)–3(i)], which protect against errors quadratic in \hat{a} or \hat{a}^\dagger [14]. The achieved fidelities are reported in Table I. To the best of our knowledge, this work appears to be the first experimental preparation of distance-3 binomial code words.

Finally, we examine the impact of incorporating robustness against motional dephasing by comparing *robust* and *nonrobust* optimized state-preparation protocols. Here, we remove duration constraints in the optimization for both pulses, and the *nonrobust* pulse is optimized without $\hat{a}^\dagger\hat{a}$ Hamiltonian terms [34]. Experimentally, we compare both protocols for binomial state $|+Z_{S=1}\rangle_{\text{bin}}$ preparation (see Fig. 4) and measure a pseudofidelity

$$\tilde{\mathcal{F}} = \frac{1}{\mathcal{N}} \sum_i \chi_{\text{exp}}(\beta_i) \chi_{\text{th}}(\beta_i), \quad (3)$$

which computes the overlap of experimental and theoretical characteristic functions [53]. Here, $\mathcal{N} = 1 / \sum_i \chi_{\text{th}}(\beta_i)^2$ is a normalization factor. This strategy provides a qualitative comparison with fewer measurements. We quantify the robustness in the presence of applied quasistatic $\delta\hat{a}^\dagger\hat{a}$ offsets, which can be associated with miscalibrations of the motional frequency. Figure 4 illustrates that the fidelity of the state generated using a *robust* pulse remains stable despite errors up to $\delta/\Omega = \pm 0.1$, while errors accumulate rapidly for the *nonrobust* pulse as $|\delta|$ increases from zero. Furthermore, the *robust* pulse achieves up to $4.8\times$ lower error for $\delta/\Omega = -0.1$. Measurements for both cases align well with theoretical predictions when incorporating state-preparation and measurement (SPAM) errors.

The main error mechanisms affecting achieved fidelities and squeezing parameters are thermal noise and motional dephasing [34]. Thermal noise results from imperfect cooling, with typically achieved average phonon occupancies of $\bar{n} = 0.05\text{--}0.1$. Motional dephasing noise arises from noise in the ion trap's rf resonator and its electronic circuit. Numerical simulations suggest that dephasing also leads to significant infidelities during the reconstruction protocol,

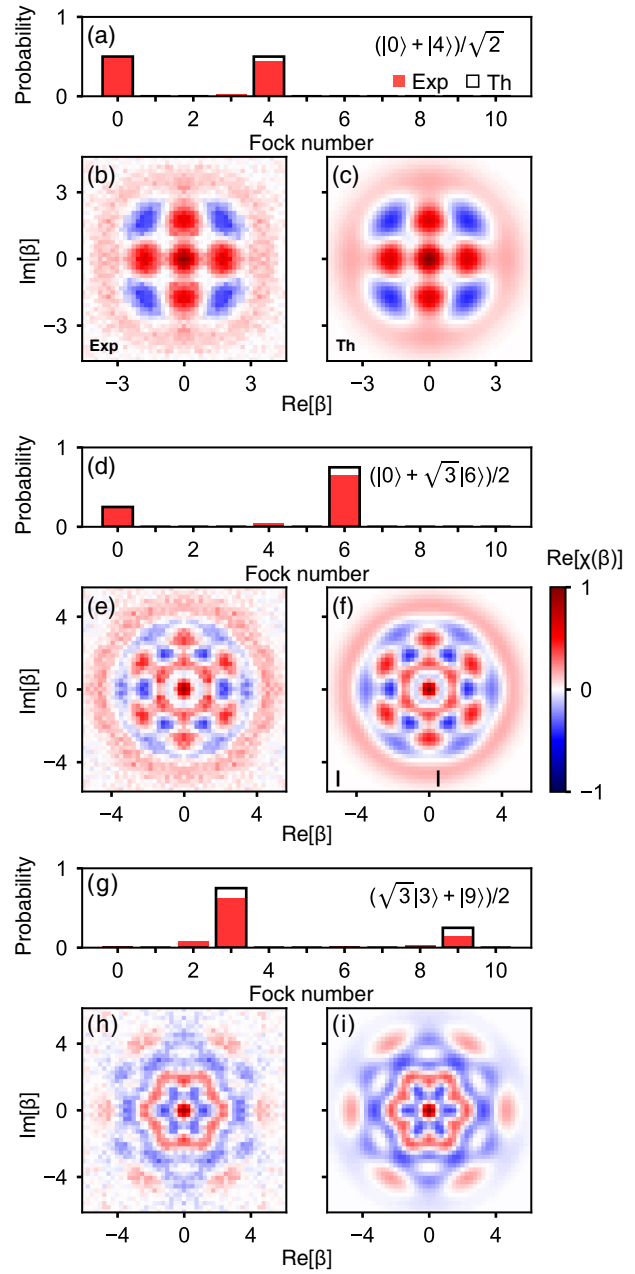


FIG. 3. Reconstructed characteristic function of binomial code words. Experimental and theoretical characteristic functions of (b),(c) $|+Z_{S=1}\rangle_{\text{bin}} = (1/\sqrt{2})(|0\rangle + |4\rangle)$, (e),(f) $|+Z_{S=2}\rangle_{\text{bin}} = \frac{1}{2}(|0\rangle + \sqrt{3}|6\rangle)$, and (h),(i) $|+Z_{S=2}\rangle_{\text{bin}} = \frac{1}{2}(\sqrt{3}|3\rangle + |9\rangle)$. (a),(d),(g) Theoretical (unshaded, black) and experimental (shaded, red) Fock number occupation probabilities, calculated from $\hat{\rho}_{\text{exp}}$. Preparation of $|+Z_{S=2}\rangle_{\text{bin}}$ begins with the ancilla qubit in the $|\uparrow\rangle$ state. The theoretical decoherence-free fidelities for each state are $\mathcal{F}_{\text{th}} \geq 0.9999$.

potentially dominating the results reported in Table I. Approximately 3%–7% of the measured characteristic function error also results from residual spin-motion entanglement, causing $\text{Re}[\chi(0)] \neq 1$ after the pulse. This can be mitigated by a midcircuit measurement before the

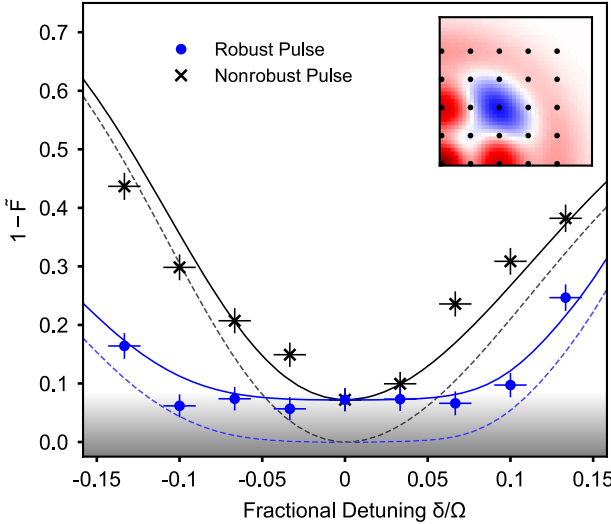


FIG. 4. Robustness against errors in motional frequency in preparing a binomial state. Experimental offsets are engineered in software by adding symmetric frequency shifts to the red- and blue-sideband fields. Pseudofidelity measurements indicate that the *robust* pulse (blue, $T = 1073 \mu\text{s}$) is less sensitive to noise than the *nonrobust* pulse (black, $T = 759 \mu\text{s}$). The inset shows the top right quadrant of the $(|0\rangle + |4\rangle)/\sqrt{2}$ binomial state's characteristic function, and black markers indicate the 5×5 points that were sampled to measure $\tilde{\mathcal{F}}$ [Eq. (3)]. The dashed theory line is obtained from numerical simulations. The solid theory line includes a scaling correction to account for infidelities during preparation and reconstruction to indicate the qualitative agreements between SPAM-adjusted theoretical results and experiment. The gray shaded region depicts the SPAM error floor, which we define by the fidelity of the robust pulse at $\delta = 0$. The y error bars indicate the uncertainty from quantum projection noise (500 repetitions). The x error bars are the uncertainty of the applied frequency offset due to drifts of the motional mode.

reconstruction pulse; we have opted against this due to substantial motional dephasing-induced errors during measurement.

In summary, we have demonstrated a deterministic protocol for generating a wide range of high-fidelity bosonic states relevant to QEC using numerically optimized and error-robust pulses. Our scheme only requires phase modulation of first-order red- and blue-sideband transitions, compatible with conventional experimental techniques. This approach surpasses gate-based methods [26,54] as pulse-level optimization enables higher theoretical fidelities for a given duration [34].

The protocol's versatility, robustness to dephasing, and the quality of the states demonstrated in this work suggest that this method is promising for bosonic QEC. Our achieved squeezed state only uses first-order sideband interactions and offers an alternative to previous trapped-ion demonstrations [55–57]. Furthermore, the distance-3 binomial code words created by our protocol demonstrate the experimental feasibility of implementing logical codes

that can simultaneously protect against boson loss, gain, and dephasing events [14]. Our GKP states show high logical fidelities and squeezings and may also be useful for quantum sensing of displacements [51], opening new opportunities in precision measurement.

Acknowledgments—We thank Thomas Smith for helpful discussions surrounding GKP and binomial codes. We were supported by the U.S. Office of Naval Research Global (N62909-20-1-2047), the U.S. Army Research Office Laboratory for Physical Sciences (W911NF-21-1-0003), the U.S. Air Force Office of Scientific Research (FA2386-23-1-4062), the U.S. Intelligence Advanced Research Projects Activity (W911NF-16-1-0070), Lockheed Martin, the Sydney Quantum Academy (A. D. R., M. J. M., V. G. M., and T. R. T.), the University of Sydney Postgraduate Award scholarship (V. G. M.), Australian Government Research Training Program scholarship (X. C. K.), the Australian Research Council, and H. and A. Harley.

Data availability—The experimental data are available in an online repository [58].

- [1] M. A. Nielsen and I. L. Chuang, *Quantum Computation and Quantum Information* (Cambridge University Press, Cambridge, England, 2000).
- [2] R. Raussendorf and J. Harrington, Fault-tolerant quantum computation with high threshold in two dimensions, *Phys. Rev. Lett.* **98**, 190504 (2007).
- [3] A. G. Fowler, M. Mariantoni, J. M. Martinis, and A. N. Cleland, Surface codes: Towards practical large-scale quantum computation, *Phys. Rev. A* **86**, 032324 (2012).
- [4] C. Ryan-Anderson, J. Bohnet, K. Lee, D. Gresh, A. Hankin, J. Gaebler, D. Francois, A. Chernoguzov, D. Lucchetti, N. Brown, T. Gatterman, S. Halit, K. Gilmore, J. Gerber, B. Neyenhuis, D. Hayes, and R. Stutz, Realization of real-time fault-tolerant quantum error correction, *Phys. Rev. X* **11**, 041058 (2021).
- [5] L. Egan, D. M. Debroy, C. Noel, A. Risinger, D. Zhu, D. Biswas, M. Newman, M. Li, K. R. Brown, M. Cetina, and C. Monroe, Fault-tolerant control of an error-corrected qubit, *Nature (London)* **598**, 281 (2021).
- [6] Y. Zhao *et al.*, Realization of an error-correcting surface code with superconducting qubits, *Phys. Rev. Lett.* **129**, 030501 (2022).
- [7] S. Krinner, N. Lacroix, A. Remm, A. D. Paolo, E. Genois, C. Leroux, C. Hellings, S. Lazar, F. Swiadek, J. Herrmann, G. J. Norris, C. K. Andersen, M. Müller, A. Blais, C. Eichler, and A. Wallraff, Realizing repeated quantum error correction in a distance-three surface code, *Nature (London)* **605**, 669 (2022).
- [8] E. H. Chen, T. J. Yoder, Y. Kim, N. Sundaresan, S. Srinivasan, M. Li, A. D. Córcoles, A. W. Cross, and M. Takita, Calibrated decoders for experimental quantum error correction, *Phys. Rev. Lett.* **128**, 110504 (2022).

- [9] R. Acharya *et al.*, Suppressing quantum errors by scaling a surface code logical qubit, *Nature (London)* **614**, 676 (2023).
- [10] F. H. E. Watson and S. D. Barrett, Logical error rate scaling of the toric code, *New J. Phys.* **16**, 093045 (2014).
- [11] S. Lloyd and S. L. Braunstein, Quantum computation over continuous variables, *Phys. Rev. Lett.* **82**, 1784 (1999).
- [12] S. L. Braunstein and P. van Loock, Quantum information with continuous variables, *Rev. Mod. Phys.* **77**, 513 (2005).
- [13] D. Gottesman, A. Kitaev, and J. Preskill, Encoding a qubit in an oscillator, *Phys. Rev. A* **64**, 012310 (2001).
- [14] M. H. Michael, M. Silveri, R. Brieler, V. V. Albert, J. Salmilehto, L. Jiang, and S. Girvin, New class of quantum error-correcting codes for a bosonic mode, *Phys. Rev. X* **6**, 031006 (2016).
- [15] M. Mirrahimi, Z. Leghtas, V. V. Albert, S. Touzard, R. J. Schoelkopf, L. Jiang, and M. H. Devoret, Dynamically protected cat-qubits: A new paradigm for universal quantum computation, *New J. Phys.* **16**, 045014 (2014).
- [16] C. Flühmann, T. L. Nguyen, M. Marinelli, V. Negnevitsky, K. Mehta, and J. P. Home, Encoding a qubit in a trapped-ion mechanical oscillator, *Nature (London)* **566**, 513 (2019).
- [17] W. Wang, Y. Wu, Y. Ma, W. Cai, L. Hu, X. Mu, Y. Xu, Z.-J. Chen, H. Wang, Y. P. Song, H. Yuan, C.-L. Zou, L.-M. Duan, and L. Sun, Heisenberg-limited single-mode quantum metrology in a superconducting circuit, *Nat. Commun.* **10**, 4382 (2019).
- [18] K. C. McCormick, J. Keller, S. C. Burd, D. J. Wineland, A. C. Wilson, and D. Leibfried, Quantum-enhanced sensing of a single-ion mechanical oscillator, *Nature (London)* **572**, 86 (2019).
- [19] A. Eickbusch, V. Sivak, A. Z. Ding, S. S. Elder, S. R. Jha, J. Venkatraman, B. Royer, S. M. Girvin, R. J. Schoelkopf, and M. H. Devoret, Fast universal control of an oscillator with weak dispersive coupling to a qubit, *Nat. Phys.* **18**, 1464 (2022).
- [20] M. Kudra, M. Kervinen, I. Strandberg, S. Ahmed, M. Scigliuzzo, A. Osman, D. P. Lozano, M. O. Tholén, R. Borgani, D. B. Haviland, G. Ferrini, J. Bylander, A. F. Kockum, F. Quijandría, P. Delsing, and S. Gasparinetti, Robust preparation of Wigner-negative states with optimized snap-displacement sequences, *PRX Quantum* **3**, 030301 (2022).
- [21] S. Konno, W. Asavanant, F. Hanamura, H. Nagayoshi, K. Fukui, A. Sakaguchi, R. Ide, F. China, M. Yabuno, S. Miki, H. Terai, K. Takase, M. Endo, P. Marek, R. Filip, P. van Loock, and A. Furusawa, Logical states for fault-tolerant quantum computation with propagating light, *Science* **383**, 289 (2024).
- [22] R. W. Heeres, P. Reinhold, N. Ofek, L. Frunzio, L. Jiang, M. H. Devoret, and R. J. Schoelkopf, Implementing a universal gate set on a logical qubit encoded in an oscillator, *Nat. Commun.* **8**, 94 (2017).
- [23] N. Ofek, A. Petrenko, R. Heeres, P. Reinhold, Z. Leghtas, B. Vlastakis, Y. Liu, L. Frunzio, S. M. Girvin, L. Jiang, M. Miriam, M. H. Devoret, and R. J. Schoelkopf, Extending the lifetime of a quantum bit with error correction in superconducting circuits, *Nature (London)* **536**, 441 (2016).
- [24] L. Hu, Y. Ma, W. Cai, X. Mu, Y. Xu, W. Wang, Y. Wu, H. Wang, Y. Song, C. Zou, S. M. Girvin, L.-M. Duan, and L. Sun, Quantum error correction and universal gate set operation on a binomial bosonic logical qubit, *Nat. Phys.* **15**, 503 (2019).
- [25] P. Campagne-Ibarcq, A. Eickbusch, S. Touzard, E. Zalys-Geller, N. E. Frattini, V. V. Sivak, P. Reinhold, S. Puri, S. Shankar, R. J. Schoelkopf, L. Frunzio, M. Mirrahimi, and M. H. Devoret, Quantum error correction of a qubit encoded in grid states of an oscillator, *Nature (London)* **584**, 368 (2020).
- [26] B. d. Neeve, T.-L. Nguyen, T. Behrle, and J. P. Home, Error correction of a logical grid state qubit by dissipative pumping, *Nat. Phys.* **18**, 296 (2022).
- [27] V. V. Sivak, A. Eickbusch, B. Royer, S. Singh, I. Tsoutsios, S. Ganjam, A. Miano, B. L. Brock, A. Z. Ding, L. Frunzio, S. M. Girvin, R. J. Schoelkopf, and M. H. Devoret, Real-time quantum error correction beyond break-even, *Nature (London)* **616**, 50 (2023).
- [28] Z. Ni, S. Li, X. Deng, Y. Cai, L. Zhang, W. Wang, Z.-B. Yang, H. Yu, F. Yan, S. Liu, C.-L. Zou, L. Sun, S.-B. Zheng, Y. Xu, and D. Yu, Beating the break-even point with a discrete-variable-encoded logical qubit, *Nature (London)* **616**, 56 (2023).
- [29] D. Lachance-Quirion, M.-A. Lemonde, J. O. Simoneau, L. St-Jean, P. Lemieux, S. Turcotte, W. Wright, A. Lacroix, J. Fréchette-Viens, R. Shillito, F. Hopfmüller, M. Tremblay, N. E. Frattini, J. C. Lemire, and P. St-Jean, Autonomous quantum error correction of Gottesman-Kitaev-Preskill states, *Phys. Rev. Lett.* **132**, 150607 (2024).
- [30] N. C. Menicucci, Fault-tolerant measurement-based quantum computing with continuous-variable cluster states, *Phys. Rev. Lett.* **112**, 120504 (2014).
- [31] K. Fukui, A. Tomita, A. Okamoto, and K. Fujii, High-threshold fault-tolerant quantum computation with analog quantum error correction, *Phys. Rev. X* **8**, 021054 (2018).
- [32] H. Ball, M. J. Biercuk, A. R. R. Carvalho, J. Chen, M. Hush, L. A. D. Castro, L. Li, P. J. Liebermann, H. J. Slatyer, C. Edmunds, V. Frey, C. Hempel, and A. Milne, Software tools for quantum control: Improving quantum computer performance through noise and error suppression, *Quantum Sci. Technol.* **6**, 044011 (2021).
- [33] D. J. Wineland, C. Monroe, W. M. Itano, D. Leibfried, B. E. King, and D. M. Meekhof, Experimental issues in coherent quantum-state manipulation of trapped atomic ions, *J. Res. Natl. Inst. Stand. Technol.* **103**, 259 (1998).
- [34] See Supplemental Material at <http://link.aps.org/supplemental/10.1103/PhysRevLett.133.050602>, which includes Refs. [35–42], for additional information about the experimental methods, numerical optimization, and analysis.
- [35] S. Diamond and S. Boyd, CVXPY: A Python-embedded modeling language for convex optimization, *J. Mach. Learn. Res.* **17**, 1 (2016), <http://jmlr.org/papers/v17/15-408.html>.
- [36] I. Strandberg, Simple, reliable, and noise-resilient continuous-variable quantum state tomography with convex optimization, *Phys. Rev. Appl.* **18**, 044041 (2022).
- [37] I. Tzitrin, J. E. Bourassa, N. C. Menicucci, and K. K. Sabapathy, Progress towards practical qubit computation using approximate Gottesman-Kitaev-Preskill codes, *Phys. Rev. A* **101**, 032315 (2020).

- [38] A. L. Grimsmo and S. Puri, Quantum error correction with the Gottesman-Kitaev-Preskill code, *PRX Quantum* **2**, 020101 (2021).
- [39] S. Haroche and J.-M. Raimond, *Exploring the Quantum* (Oxford University Press, New York, 2006).
- [40] M. H. Shaw, A. C. Doherty, and A. L. Grimsmo, Stabilizer subsystem decompositions for single- and multimode Gottesman-Kitaev-Preskill codes, *PRX Quantum* **5**, 010331 (2024).
- [41] M. H. Shaw, A. C. Doherty, and A. L. Grimsmo, Logical gates and read-out of superconducting Gottesman-Kitaev-Preskill qubits, [arXiv:2403.02396](https://arxiv.org/abs/2403.02396).
- [42] J. Hastrup, K. Park, R. Filip, and U. L. Andersen, Unconditional preparation of squeezed vacuum from Rabi interactions, *Phys. Rev. Lett.* **126**, 153602 (2021).
- [43] C. K. Law and J. H. Eberly, Arbitrary control of a quantum electromagnetic field, *Phys. Rev. Lett.* **76**, 1055 (1996).
- [44] Q-CTRL, Boulder Opal, <https://q-ctrl.com/boulder-opal> (2023).
- [45] R. J. MacDonell, T. Navickas, T. F. Wohlers-Reichel, C. H. Valahu, A. D. Rao, M. J. Millican, M. A. Currington, M. J. Biercuk, T. R. Tan, C. Hempel, and I. Kassal, Predicting molecular vibronic spectra using time-domain analog quantum simulation, *Chem. Sci.* **14**, 9439 (2023).
- [46] C. H. Valahu, V. C. Olaya-Agudelo, R. J. MacDonell, T. Navickas, A. D. Rao, M. J. Millican, J. B. Pérez-Sánchez, J. Yuen-Zhou, M. J. Biercuk, C. Hempel, T. R. Tan, and I. Kassal, Direct observation of geometric-phase interference in dynamics around a conical intersection, *Nat. Chem.* **15**, 1503 (2023).
- [47] C. Flühmann and J. Home, Direct characteristic-function tomography of quantum states of the trapped-ion motional oscillator, *Phys. Rev. Lett.* **125**, 043602 (2020).
- [48] S. Ahmed, C. S. Muñoz, F. Nori, and A. F. Kockum, Quantum state tomography with conditional generative adversarial networks, *Phys. Rev. Lett.* **127**, 140502 (2021).
- [49] X. C. Kolesnikow, R. W. Bomantara, A. C. Doherty, and A. L. Grimsmo, Gottesman-Kitaev-Preskill state preparation using periodic driving, *Phys. Rev. Lett.* **132**, 130605 (2024).
- [50] B. Efron and R. Tibshirani, *An Introduction to the Bootstrap* (Chapman and Hall/CRC, London, 1994).
- [51] K. Duivenvoorden, B. M. Terhal, and D. Weigand, Single-mode displacement sensor, *Phys. Rev. A* **95**, 012305 (2017).
- [52] M. H. Michael, M. Silveri, R. T. Brierley, V. V. Albert, J. Salmilehto, L. Jiang, and S. M. Girvin, New class of quantum error-correcting codes for a bosonic mode, *Phys. Rev. X* **6**, 031006 (2016).
- [53] R. P. Rundle and M. J. Everitt, Overview of the phase space formulation of quantum mechanics with application to quantum technologies, *Adv. Quantum Technol.* **4**, 2100016 (2021).
- [54] J. Hastrup, K. Park, J. B. Brask, R. Filip, and U. L. Andersen, Measurement-free preparation of grid states, *npj Quantum Inf.* **7**, 17 (2021).
- [55] D. M. Meekhof, C. Monroe, B. E. King, W. M. Itano, and D. J. Wineland, Generation of nonclassical motional states of a trapped atom, *Phys. Rev. Lett.* **76**, 1796 (1996).
- [56] D. Kienzler, H.-Y. Lo, B. Keitch, L. de Clercq, F. Leupold, F. Lindenfelser, M. Marinelli, V. Negnevitsky, and J. P. Home, Quantum harmonic oscillator state synthesis by reservoir engineering, *Science* **347**, 53 (2015).
- [57] S. C. Burd, R. Srinivas, J. J. Bollinger, A. C. Wilson, D. J. Wineland, D. Leibfried, D. H. Slichter, and D. T. C. Allcock, Quantum amplification of mechanical oscillator motion, *Science* **364**, 1163 (2019).
- [58] V. G. Matsos, C. H. Valahu, T. Navickas, A. D. Rao, M. J. Millican, X. C. Kolesnikow, M. J. Biercuk, and T. R. Tan, Robust and deterministic preparation of bosonic logical states in a trapped ion, [10.5281/zenodo.12741298](https://doi.org/10.5281/zenodo.12741298) (2023).